MEASURING GAS INTERDIFFUSION AND CO_2 SEQUESTRATION IN HELESHAW CELL

A Thesis

Presented to the Faculties of the Graduate School

of Cornell University

In Partial Fulfillment of the Requirements for the Degree of

Master of Science

by

Yushi Zhao

May 2013

ABSTRACT

CO_2 sequestration is receiving attention presently because it is one way to minimize the climate impact of continued use of fossil fuels. This thesis experimentally investigates how CO_2, injected into fractures within gas shales, could be stored by diffusively exchanging with methane in the shale matrix. Experiments are carried out in a HeleShaw style apparatus. The apparatus consists of an open square channel with dimensions of 1cm x 1cm x 100cm long that is connected to 19 of 5 cm wide and 100 cm long diffusion slit with 2mm aperture. Gas passed into the channel diffuses into the slit, simulating diffusion into the shale matrix from the fractures into which CO_2 is injected. The apparatus was filled with methane and CO_2 was then injected in the channel. The fraction of CO_2 was determined from the difference between the moles of CO_2 injected and emitted. The effects of gravity were assessed by changing the orientation of the diffusion slit. Slower flow rates result in higher sequestration because there is more time for CO_2 to diffuse into the slit. Sequestration is increased if the slit is oriented such that CO_2 can drain into the slit under gravity. Because of the very low permeability of shale, gravity effects are not expected to be important in shales, but are important in our experiments. Models of the sequestration reproduce the HeleShaw Cell gaseous diffusion experiments quite well when gravity is not a factor in the experiments. These models allow translation of the laboratory results to field tests.

ACKNOWLEDGEMENTS

I would like to thank firstly, KAUST-CU Center for Energy and Sustainability for facility support for my research work. I would like to thank Dr. Cathles for his diligent guidance and advisory on my research. Dr. Cathles keeps me on my feet, tracks down my progress and keeps me motivated in all circumstances. I would also like to thank my secondary advisor Dr. James R. Engstrom serving in my committee and for his valuable inputs in my research work throughout the program.

I would like to thank my colleagues and group members for providing such a harmonious atmosphere to work in, and lending out helping hands when I needed. I would like to thank my formal colleague Francis Mulcahy, for ordering and fabricating the hardware with the machine shop. I thank all the people and institutions which assisted me in my research, namely Shivaun Archer of Cornell Weill Hall Student Lab, John Grazul of Cornell CCMR, Panagiotis Dallas from Dr. Emmanuel P. Giannelis' group, Lin Chen and Yisheng Xu from Dr. Christopher K. Ober's group; Cornell CNF, Cornell Clark Hall Machine Shop, Special Glass Product Inc, CO_2meters.com; Thank you Brenda Fisher, Dave Jung, Celia Szczepura, Savannah Sawyer, Amy Colvin, for training, assisting, and keeping everything running.

Thank you my family and friends for being super supportive.

TABLE OF CONTENTS

LIST OF FIGURES

LIST OF TABLES

PREFACE

In low permeability gas shale formations, gas (primarily methane) is naturally stored in the pores and fractures of the reservoir rock, as well as adsorbed within the organic material contained within the rock structure of the formation. As carbon dioxide (CO_2)is injected into a gas shale formation, the CO_2 can displace the adsorbed methane. In addition to enhancing gas recovery (EGR), the CO_2 can be permanently stored, or sequestered, in the pore space.

The project of which this laboratory study is a part investigates how CO_2 injected into fractures within gas shales will diffusively exchange with methane in the matrix, and how measuring this diffusive intermixing might provide added information of how successfully the injected CO_2 might be stored in the shale.

This master's thesis constitutes a report of analogue laboratory experiments which I carried out that were designed to elucidate how CO_2 will diffuse into air and into CH_4 contained in the shale matrix when the CO_2 is introduced into fractures in the shale. The laboratory experiments are carried out in a meter-long Hele-Shaw cell at atmospheric temperature and pressure. The Hele-Shaw cell is constructed of acrylic glass that does not react with CO_2 or methane. We conducted the diffusion experiments at different injection rates and in different orientations of the apparatus in which the injected gas was either gravitationally stable or unstable. The total fraction of CO_2 sequestered in the shale was the measured parameter of principle interest. The experiments are

interpreted by a simple model which allows the results to be translated to field experiments.

The experiments indicate that the methods proposed have the potential to give an early assessment of how successfully CO_2 could be sequestered in gas shale formations. Areas that need further investigation are identified.

CHAPTER 1

INTRODUCTION

Fractures, both naturally occurring and induced, are a principal factor controlling the volume and rate of natural gas production from the shales, the amount of gas that can be permanently stored in gas shale formations, and the risk associated with that storage.

Shales are comprised of thin laminations of sediment with slightly different grain size and different proportions of carbonate, sand, clay, and organic carbon. The shales are faulted and jointed both on a large (meters to tens of meters) and small (single strata) scale. Different lamina can be fractured to very different degrees. Shale permeability is very low, but complex connections between the most permeable lamina and fractures provide some permeability. This permeability increases strongly with fluid pressure and deformation, an extreme case being when the shale is hydraulically fractured. Thus, it is possible to inject CO_2 into a shale formation, and it is possible that, considering diffusion away from the fractures and permeable laminae, the storage efficiency (e.g., the fraction of the pore space of the shale filled with CO_2) might be high.

Depleted shale gas reservoirs could be an economic way to sequester carbon because methane could be recovered as CO_2 is stored. In low permeability shale formations, gas is stored in the pores and fractures of the reservoir rock, as

well as adsorbed within the organic material contained within the rock structure of the formation. As CO_2 is injected into a depleted gas shale reservoir, it is possible for the CO_2 to adsorb onto the shale and displace adsorbed methane. As methane desorbs from the reservoir rock, the CO_2 is sequestered in the reservoir pore space as well as adsorbed onto the shale, and the displaced methane is produced at the well head. This process, known as enhanced gas recovery (EGR), is widely practiced in coal seams in the San Juan Basin of New Mexico (Nuttall, 2005). It is believed that the mechanisms for EGR and CO_2 storage in coal seams and gas shales are similar.

The purpose of this thesis is to determine if the inter-diffusion of CO_2 and methane could measure the uniformity with which CO_2 can be injected into a methane bearing shale. The experiment uses a Hele-Shaw cell modified to have a permeable core channel adjacent to a narrow compartmented slit into which CO_2 from the channel can diffuse. In this experiment, adsorption is not addressed. Because the gases differ in density, we run experiments with the CO_2 channel at the top and bottom of the vertical diffusion slit, as well as experiments with light gas and heavy gas filling the diffusional slit of the apparatus.

Some frequently used terms used with regard to the experiments described in this thesis include:

- **Orientation**: This refers to whether the core channel of the Hele-Shaw apparatus which receives and transmits most of the injected fluid is at the top, bottom, or at side of the diffusion cell. A stable orientation is one in which the core channel is on the bottom when a heavy gas (e.g., heavier than the gas in the diffusion slit) is injected, or one in which the core channel is on the top and a light gas is injected. An unstable orientation is one in which the opposite is the case.

- **Configuration variation:** This refers to whether a heavier channel gas is diffusing into a lighter slit (matrix) gas, or a lighter channel gas is diffusing into a heavier slit gas.

- **Flow rate:** This refers to the injection flow rate into the core channel. Flow rates vary between 1.8 cubic centimeters (cc) /Minute to 5.2 cc/Minute.

- **Storage Fraction:** The fraction of the total apparatus pore volume filled with the injected gas. Also referred as sequestration.

CHAPTER 2

PRIOR WORKS

Diffusion is one of the most fundamental phenomena of nature. According to Fick's Law, physical diffusion will occur where there is a concentration gradient. The diffusion flux is inversely proportional to the gradient, and the diffusion is from higher to lower concentrations. Thermal diffusion is also a fundamental phenomenon of thermodynamics. At atomistic level, diffusion is the result of a random walk of the diffusing particles, while are self-propelled by thermal energy.

In 1831, Thomas Graham carried out the first systematic experimental study of diffusion. In 1858, Rudolf Clausius introduced the concept of mean free path; while James Clerk Maxwell at the same time developed the first atomistic theory if transport processes in gases. In 1867, he derived the coefficient of diffusion of CO_2 in air. Carslaw and Jaeger (1959) worked on the mathematics of diffusion in the early 20th century .

In 1920, George de Hevesy measured the self-diffusion of lead in liquids and solids with radioisotopes. CO_2 diffusing into CH_4 can be thought as the self diffusion of CO_2 plus the self diffusion of methane. Furthermore, in 1971, Weissman and DuBro documented new values of D_{12} for the CO_2-CH_4 system obtained using a two-bulb system and they demonstrated that it is possible to obtain values of D_{12} from the viscosity η_{mix}, of mixtures of CO_2 and CH_4. Fluid

diffusion is described by the Stokes-Einstein's Equation as a function of viscosity, Boltzmann's constant, and particle size.

The definitive review of the modern theory, measurement techniques, and published experimental data is Marrero and Mason (1972). It is a major contribution to the current literature dealing with gaseous diffusion of binary gas mixtures (Sherwood, Pigford, and Wilke, 1975). Chapman and Cowling (1970) added first and second order approximations of gaseous diffusion coefficients in the same period. The estimation of our gaseous diffusion coefficients and its second order corrections are based on their semi-empirical formulas and tabulations of diffusion values.

A Hele-Shaw flow apparatus, named after Henry Selby Hele-Shaw, is an apparatus in which Stokes flow occurs between two parallel flat plates separated by a small gap where the Reynolds number is far less than one. We designed our lab experimental apparatus based the Hele-Shaw device used to investigate two-dimensional flow in porous media. The thickness of the Hele-Shaw cells is usually a few millimeters (Paterson, 1981). Our modified Hele-Shaw cell allows us to simulate CO_2 sequestration in a depleted gas shale reservoir experimentally.

The Peclet Number, named after Jean Claude Eugene Peclet, is a dimensionless number consisting of the ratio between the advection rate of a physical quantity and the rate of diffusion of the same quantity driven by an appropriate gradient. The Inverse Peclet Number, which we use in this study, is

the ratio of diffusion to the rate of flow advection. A Cornell graduate student has carried out a systematic study of Inverse Peclet Number controlling the dual tracer separation of aqueous diffusion scheme (Subramanian, Li and Cathles, 2012).

Both lateral and longitudinal dispersion are taken into account in our modeling interpretation of the experimental results. As shown in Figure 1, the flow velocity in a circular pipe is higher in the center of the tube (Evans and Kenney, 1965) and slower nearer the tube wall. This can cause the early (relative to the average velocity of the fluid through the tube) arrival of injected fluid and cause mixing. This phenomenon is called dispersion. Figure set 1b illustrates the early arrival and the effects of dispersive mixing.

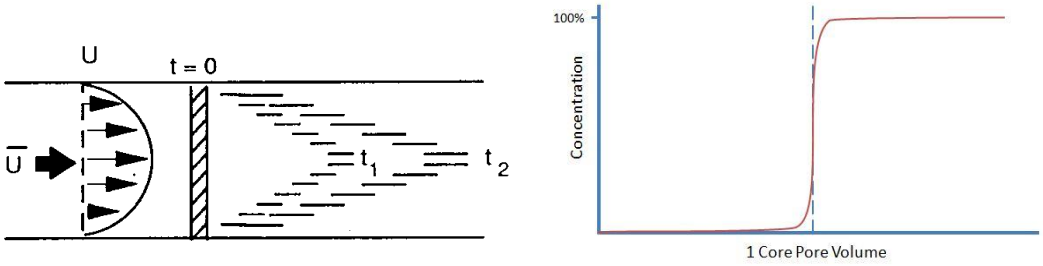

Figure 1: (a) Illustration of how the velocity profile in a tube can produce. (b) Illustration of the impact of dispersion on the effluent from a tube with a volume of 1 core pore volume.

Gaseous Diffusion Theory

Gaseous diffusion is treated differently from fluid diffusion. Because the molecules are spaced far apart in a gaseous mixture, the equation governing molecular diffusion in a gaseous phase involves mean free path and collisions of molecules. Gaseous diffusion is also very sensitive to pressure and temperature gradients in the system. The assumption for the gases and their diffusion properties are that gas molecules behave like an elastic solid sphere. The motion of colliding molecules can be described under the scheme of classical physics (there is no quantum effect). Molecules move in random directions with great void space around them. The molecules do not react, and do not show attraction or repulsion between themselves. Only binary collisions occur. Molecular forces operate only through the fixed center of molecules.

Though methane and CO_2 do not behave like ideal gases at higher pressures and low temperature, at room temperature of 298 K and 1 atmosphere pressure the behavior of the gases involved in our experiments are very close to ideal gases. If we calculate the difference between the Ideal Gas Law and Van Der Waals Equation of Gaseous State for real gases the difference is 0.2%, which is far less significant than other errors of our experiments.

Gaseous Diffusion Coefficients

The gaseous diffusion coefficients have been measured in many gas pairs. We employed the gaseous diffusion coefficients of available gas pairs, because they

are recorded from experiments and thought to be more accurate than semi-empirical correlations of experimental data or empirical estimates. However, we do use some of the empirical equations to estimate the diffusion coefficients of our gas pairs if the data are not available at our range of conditions. In addition, we take into account a second order correction that takes into account concentration differences in the gas mixtures.

With the assumptions mentioned, the first order estimation of the diffusion constants of binary gas mixtures by Hirschfelder, Curtiss and Bird (1964) is:

$$D_{12} = \frac{0.001858T^{3/2}(\frac{1}{M_1} + \frac{1}{M_2})^{1/2}}{P{\sigma_{12}}^2\Omega_D} \ cm^2/sec$$

Where T = Temperature in Kelvin.
M_1 and M_2 = the molecular weights of constituents 1 and 2
P = absolute pressure in atm
Ω_D = collision integral, $f(kT/\varepsilon_{12})$; values can be found in the cited work.
k = Boltzmann's constant
σ_{12} = dimension of cross sections.
ε_{12} = Lennard-Jones force constants for the binary pair.

The last two constants are obtained from the corresponding values for the pure substances using combination rules:

$$\frac{\varepsilon_{12}}{k} = (\frac{\varepsilon_1}{k}\frac{\varepsilon_2}{k})^{1/2}$$

$$\sigma_{12} = \frac{1}{2}(\sigma_1 + \sigma_2)$$

If values of $\frac{\varepsilon}{k}$ and σ are not available, they may be estimated by the following rule of approximation:

$$\frac{\varepsilon}{k} = 0.75T_c$$

$$\sigma = \frac{5}{6}{V_c}^{1/3}$$

Where T_c = critical temperature in Kelvin,
V_c = critical volume in $cm^3/g\ mole$.
σ = Lennard-Jones potential parameter, in Å

A second first order diffusion constant estimate for binary gas mixtures is from Chapman and Cowling (1970, page 258):

$$D_{12} = \frac{3}{8n_0{\sigma_{12}}^2}\sqrt{\frac{k_BT}{2\pi}\left(\frac{1}{m_1}+\frac{1}{m_2}\right)}\frac{1}{\Omega_{12}}$$

Where the number density n_0 is obtained from the ideal gas law, $n_0 = p_0/k_BT$
$\pi{\sigma_{12}}^2$ = the scattering cross section
k_B = Boltzmann's constant,
m_1 and m_2 = the molecular weights.
The calculation of Ω_{12} and σ_{12} are the same as the first method.

In both of these expressions, the first order estimate of binary gaseous mixture diffusion coefficient is not a function of the number density of individual gases, but only the total number density. Thus the diffusion coefficient is symmetric, $D_{12} = D_{21}$. To take into account for the difference in concentration of the gas species, we introduce the second-order correction to the diffusion coefficients which multiplies the first-order estimation by the following factor from Chapman and Cowling (1970, page 259-260), (Hudson 2008)

$$\frac{1}{1 - {m_1}^2/(13{m_1}^2 + 30{m_2}^2 + 16m_1m_2)}$$

Here m_1 is the molecular weight of the low concentration gas and m_2 the molecular weight of the high concentration gas. If methane and CO_2 are inter-diffusing, and methane has the lower concentration, this factor has a value of 1.0035. If CO_2 has the lower concentration, the factor is 1.045. The following table shows the correction for air (molecular weight 29), methane (molecular weight 16), and CO_2 (molecular weight 44)

low concentration m1	high concentration m2	correction
44	16	1.045
29	16	1.033
44	29	1.028
29	44	1.009
16	29	1.007
16	44	1.004

Table 1: values of second order diffusion coefficient corrections for selected gas pairs by Chapman's empirical equation.

CHAPTER 3

EXPERIMENTS

Gaseous Diffusion Experiment Apparatus Setup

Our modified Hele-Shaw flow cell consists of a core channel attached to a slit with 19 diffusion compartments as shown in Figure 2. The injected gas flows mainly in the core channel and diffuses into the diffusion slit. The compartmentalization of the slit is intended to reduce flow through it. The apparatus is constructed of acrylic glass.

The Hele-Shaw cell is 100 centimeters (cm) long. The cross section of the central core is a 1 x 1 cm square. The slit was designed to be 0.2 cm wide and the slit compartments are 5 cm wide by 28.5 cm long. From these dimensions the total core pore volume is 100 cc, and the total diffusion slit pore volume is 541.5 cc (= 28.5 cm x 0.2 cm x 5 cm x 19 slits). The total pore volume is 641.5 cc.

To check these calculated volumes the apparatus was filled with water and the water then was drained and its mass and volume were measured at three places: 1st is when the apparatus is fully filled with water, 2nd is when the water only covers the diffusion slits, and when water is totally drained out of the system. The total pore volume measured was 451 cc. Core channel pore volume is 100 cc, which suggests the diffusion slit pore volume is 351 cc. We can then back calculate the diffusion slit width by measuring the length and height of the diffusion slits, and we get 0.13 cm for the width of the diffusion slit rather than

0.2 cm as the design suggested. We used 100 cc as the core pore volume, and 450 cc as the total system pore volume in our interpretation. Machining the 19 slits for the compartments requires a very high level of precession. Uneven machined tracks can be identified with the naked eye. Therefore we concluded that the exact width of the diffusion channel was not quite even from compartment to compartment, and an average width of 1.3mm is reasonable. There was water adhering to some dead corners after draining, but we measured the volume of water injected as well as the volume recovered, and volume of water recovered is within 3 CC of that injected. Since the apparatus base and cover plate are quite thick, it is not likely that the apparatus deformed during usage. Thus we conclude the difference between observed dimension and designed dimension is due to machining imperfections, and use the measured slit volume in our interpretations.

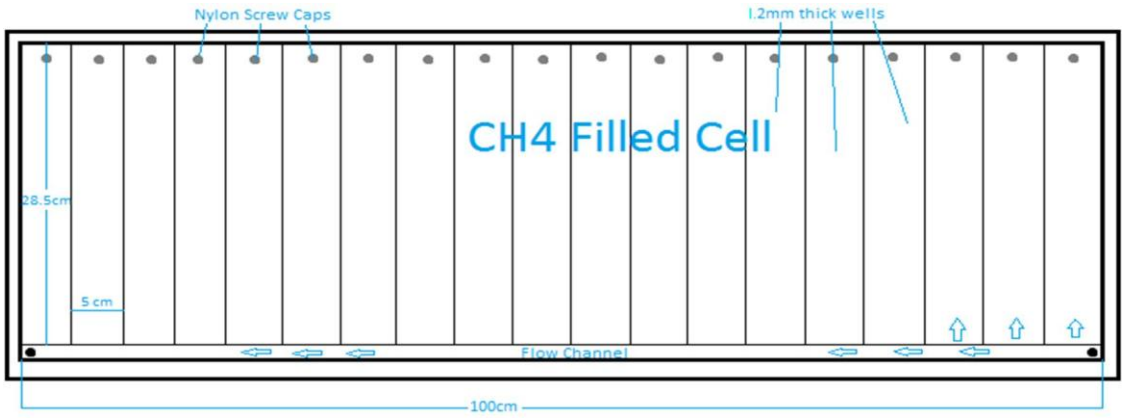

Figure 2: Hele-Shaw modified flow cell used for our gaseous diffusion experiments.

Figure 3 below shows the setup of the work station. CO_2 and methane are directly pumped from the high purity compressed gas cylinder through regulators. A three-way flow switch controls the type of gas being injected. A flow meter is attached after the switch to control the flow rate into the core channel of the Hele-Shaw cell. The range of the flow meter is 0.5 cc/min to 6 cc/min. Flow rates for our experiments are between 1.8cc/min to 5.2 cc/min (with some uncertainty due to reading and instrument errors).

Detection

Upon exiting the flow meter, the gas passes through our Hele-Shaw Core channel. The effluent gas passes through a real time, non-dispersive infrared absorption (NDIR) CO_2 sensor which is connected to a computer that captures the real time CO_2 concentration. The effluent gas is then discharged into the laboratory effluent air vent after sampling.

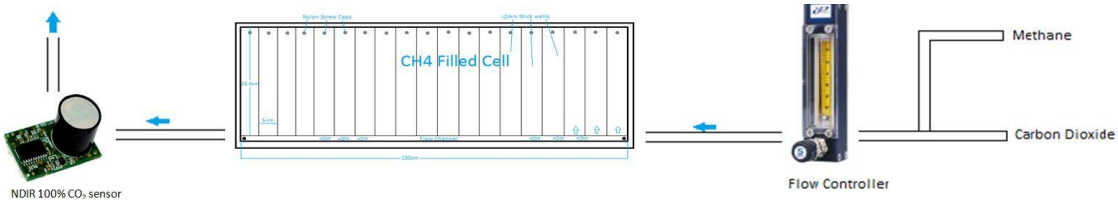

Figure 3: Schematics of the gas diffusion experiment.

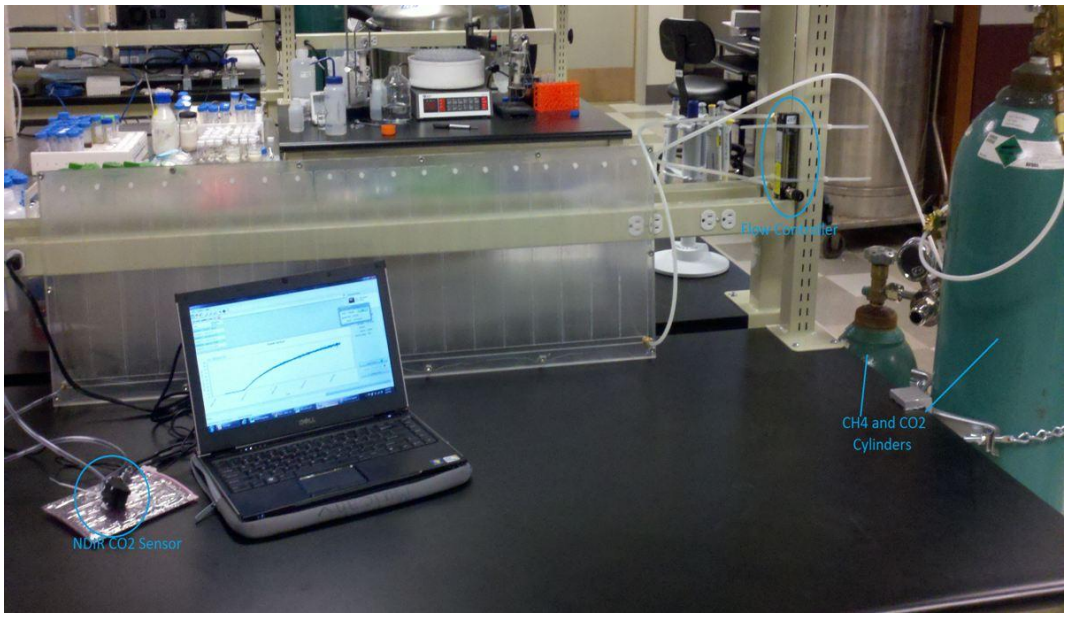

Figure 4: Gas diffusion experiment setup.

Flushing of the apparatus is an important step between every experiment. To flush the apparatus, the nylon caps of individual diffusion compartment are sequentially and separately removed, and compressed air (or CH_4 or CO_2) is injected at very high flow rate into of one side of the core channel. After flushing a minute through each compartment in this fashion, it is considered that air flow has driven out most of the residual gas from the last experiment, and the nylon caps are removed from all the slit compartments to displace the rest of the residual gas out of the apparatus by continued air injection for two or more days, depending on how clean the system was flushed the first time. Flushing can be done more efficiently if the flushing gas is introduced when the core channel is in the unstable position, since this gas then drains down (or up) into the diffusion

slit. The concentration of CO_2 is examined before every experiment to ensure the purity of the filled gas.

Once the apparatus is flushed and filled with air, CO_2 or CH_4, the experiment is begun and a contrasting gas is injected into the core pore channel at a constant rate, and the effluent CO_2 concentration is measured and recorded. Since we can only detect the CO_2 concentration, one of the gases must always be CO_2.

Sequestration Calculations

Storage fraction plots are used to calculate the amount of gas that is stored in the system permanently by diffusion into the slit. The storage fraction is the fraction of the total apparatus volume that is filled with the injected gas. Storage fraction is calculated as a function of time by the following equation:

$$f = \frac{\int_0^t Q(1 - \frac{C(t)}{C_o})dt}{V_{tot}}$$

Here f is the storage fraction, Q is the flow rate through the system, C(t)/Co is the effluent concentration divided by the injection concentration of the injected gas.

For example, consider the case where CO_2 is injected into an air filled system at 2.3 cc/minute with the core channel at the bottom in the stable

position. Figure 5 shows the effluent concentration of CO_2 as a function of time and the core pore volumes injected.

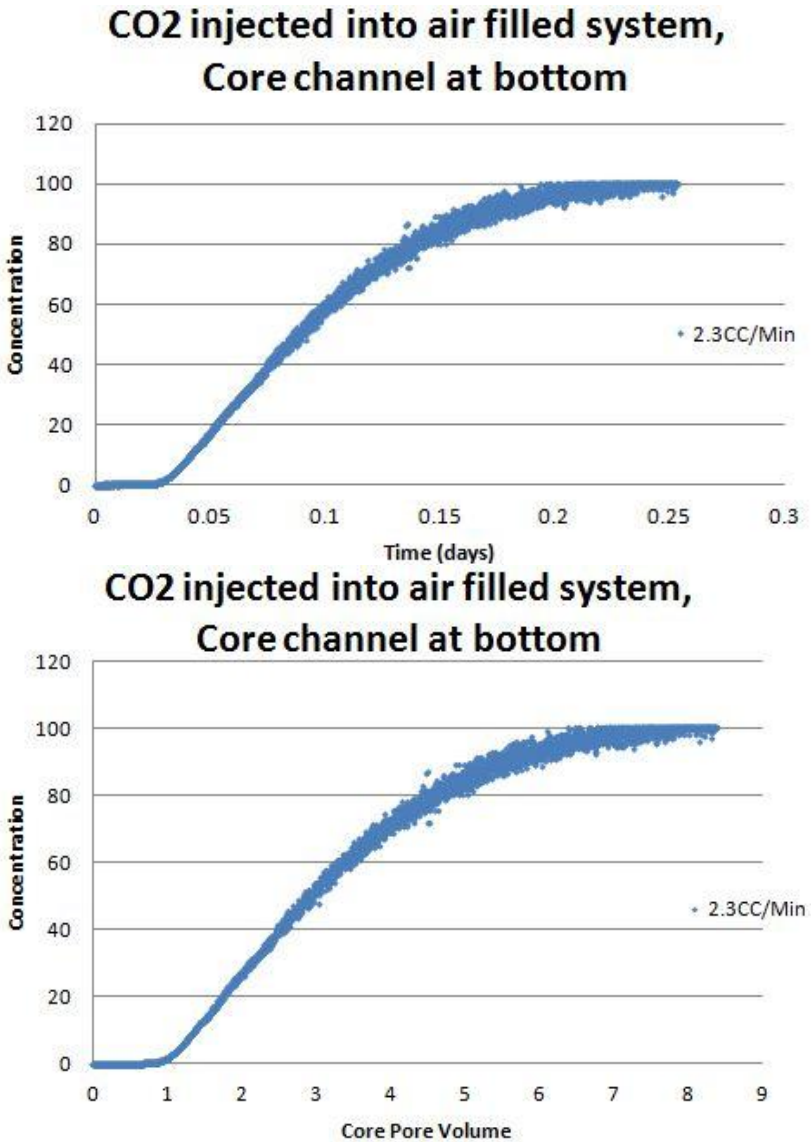

Figure 5: Effluent CO_2 concentrations as a function of time and the number of core pore volumes injected.

Figure 6a plots the fraction of air in the effluent as a function of time, and Figure 6b illustrates how increments of this curve can be multiplied by the flow

rate and summed to obtain the total CO_2 retained in the apparatus, or sequestered.

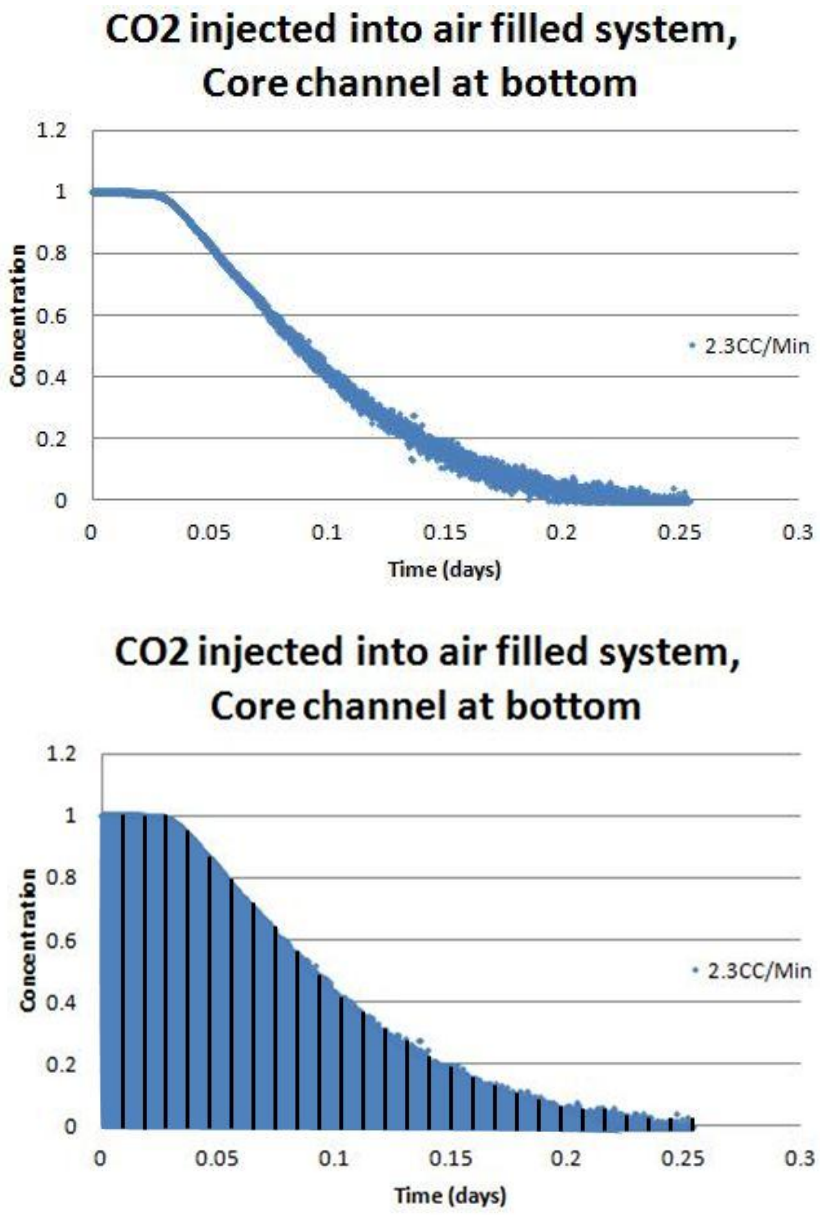

Figure 6. (a) The fraction of injected CO_2 not present in the effluent and therefore left behind in the apparatus. (b) Discrete time intervals of this curve that can be multiplied by the flow rate to obtain the increments of CO_2 sequestered over time. These increments are summed between t=0 and t to obtain the storage fraction plot shown in Figure 7.

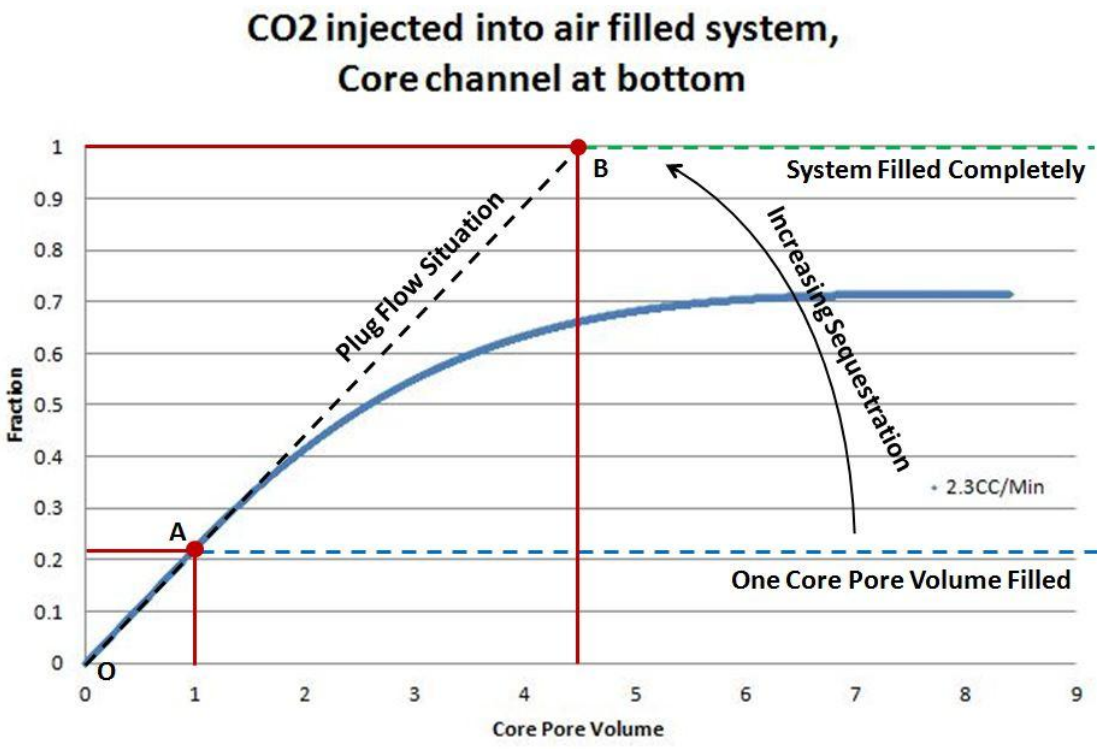

Figure 7: Storage fraction as a function of time for the experiment shown in Figure 5.

Figure 7 shows how CO_2 is sequestered in the laboratory apparatus shown in Figures 2-4 when injected at 2.3 cc/minute. Consider a few key points in this graph. We know that our core channel has pore volume of 100 cc, which is 100/450 = 0.22, or 22% of the total pore volume. If we filled the core channel completely, we will have filled 22% of the system pore volume. The red dot at point A indicates how the injection of one core pore volume of CO_2 will sequester CO_2 in 22% of the total apparatus pore volume. If we inject CO_2 into our system at a constant rate, we should see a straight line from the origin O to point A, and, if there is no diffusion from the core pore channel into the slit, this is all the CO_2 that will ever be sequestered and sequestration

curve will be flat from point A to the left edge of the graph along the bottom horizontal dotted line.

If, on the other hand, the diffusion from the channel into the slit is very fast, so that the slit is filled as the CO_2 front proceeds along the core channel, the whole apparatus will fill with CO_2 in a plug flow fashion, and the sequestration fraction will continue to increase linearly from point A to point B as 4.5 core pore volumes (the total pore volume) are injected. The sequestration fraction will rise along the slanted dashed line, and then flatten along the top horizontal dashed line when the apparatus is completely filled.

If the diffusion from the channel is not infinitely fast or slow, the sequestration curve will lie between the two extremes just discussed. The sequestration curve for the experiment in Figure 6 is shown as the blue curve in Figure 7. In this case, the sequestration increases to about 0.7 of what could be sequestered, and it then flattens in a fashion that indicates that there is very little further sequestration after about 7 core pore volumes have been injected.

Gaseous Diffusion Experiments

We have conducted three groups of experiments with the following protocols:

CO_2 Injected in an Air Filled System

After the system is flushed and filled with air as described above, we injected CO_2 and measure the effluent CO_2 concentration. Experiments are conducted in either a stable orientation (heavier gas flowing in the core channel placed below the diffusion compartments, or gravity drainage orientation) or in an unstable orientation (heavier gas flowing in the core channel placed on top of the diffusion compartments, or gravity segregation orientation) at two different flow rates: 2.3 cc/min and 5.2 cc/min (with some range of reading error and instrument error). Each experiment is repeated at least twice to assure data consistency. Data is collected for a few hours for the gas to fill the apparatus. Data collection is stopped when the effluent concentration of the injected gas reaches 100%.

CO_2 Injected in a CH_4 Filled System

After the system is flushed with CH_4 as described above, we inject CH_4 and measure the effluent CO_2 concentration to infer the concentration of CH_4 in the system. Experiments are again conducted in either a stable or unstable orientation at three different flow rates: 2 cc/min, 2.4 cc/min and 5 cc/min (with some range of reading error and instrument error). Each experiment is repeated at least twice to assure data consistency. Data is collected for the few hours that

the gas takes to fill the apparatus. Data collection is stopped when the effluent concentration of the injected gas reaches 100%.

CH_4 Injected in CO_2 Filled System

After the system is flushed with CO_2 as discussed above, CH_4 is injected into the core channel and the effluent CO_2 concentration is measured. Experiments are conducted in either the stable or unstable orientation at three different flow rates: 1.8 cc/min, 2.1 cc/min and 4.1 cc/min (with some range of reading error and instrument error). Each experiment is repeated at least twice to assure data consistency. Data is collected for the few hours it takes for the gas to fill the apparatus. Data is stopped when the effluent concentration of injected gas reaches 100%.

CHAPTER 4

Interpreting Gaseous Diffusion Experimental Results and Discussion

The results of the experiments we have performed are now presented graphically and discussed, mainly in the figure captions. Figures 8 to 11 show effluent and storage fraction plots for the injection of CO_2 into an air-filled system, methane into a CO_2-filled system, and CO_2 into a methane-filled system, for different orientations of the system. Figures 12 to 14 compare different flow rates for these systems. Figure 15 compares the effluent plots for stable orientations where the flow rate is close to 2 cc/min.

The storage plots in Figures 8 to 11 show that more of the injected gas is stored if the configuration is unstable or the injection rate slower. This is reasonable because in the unstable orientation the injected gas drains under gravity into the slit compartments. The longer residence times when injection is slower allow more time for the injected gas to diffuse into the slit.

We estimate the storage fraction in Figures 8 to 11 either when the curve plateaus or at ~8 core pore volumes. These storage numbers are posted next to the storage fraction curves and they are summarized in Table 2. The figures and Table 2 show that the largest storage fractions are produced when CH_4 is injected into a CO_2-filled system. The second largest storage is when CO_2 is injected into an air-filled system. The smallest storage fractions are attained when CO_2 is injected into a CH_4-filled system. The end-members in this distribution stand

out. Methane injected into a CO_2-filled system sequesters substantially more of the injected gas and, unlike the other cases, the storage fractions keep rising with injection beyond 8 core pore volumes. Conversely substantially less of the injected gas is stored when CO_2 is injected into a methane filled system.

.

	~5 cc/min		~2.3 cc/min		~2 cc/min	
	stable	unstable	stable	unstable	stable	unstable
$CH_4 \rightarrow CO_2$	0.70	0.70	0.70	0.72	0.72	0.75
$CO_2 \rightarrow$air	0.65	0.71	0.71	0.77		
$CO_2 \rightarrow CH_4$	0.52	0.62	0.58	0.65	0.60	0.70
	0.55/0.52		0.60/0.58		0.68/0.60	

Table 2. Summary of storage fractions at 8 core pore volumes from Figures 8-11. Storage fraction is higher for unstable orientations and for lower injection rates. Storage is highest when CH_4 is injected into a CO_2-filled system and lowest then CO_2 is injected into a CH_4-filled system. The / ## in the last row is for the flat orientation.

Figures 12 to 14 show clearly how the storage fraction increases as the injection rate decreases. Looking at the stable configuration plots in these figures it can be seen that again CH_4 injection into a CO_2-filled system is special: this case shows much less dependence on injection rate than the other cases.

Figure 15 shows CO_2 injected into CH_4 has less storage than when the other gases are injected.

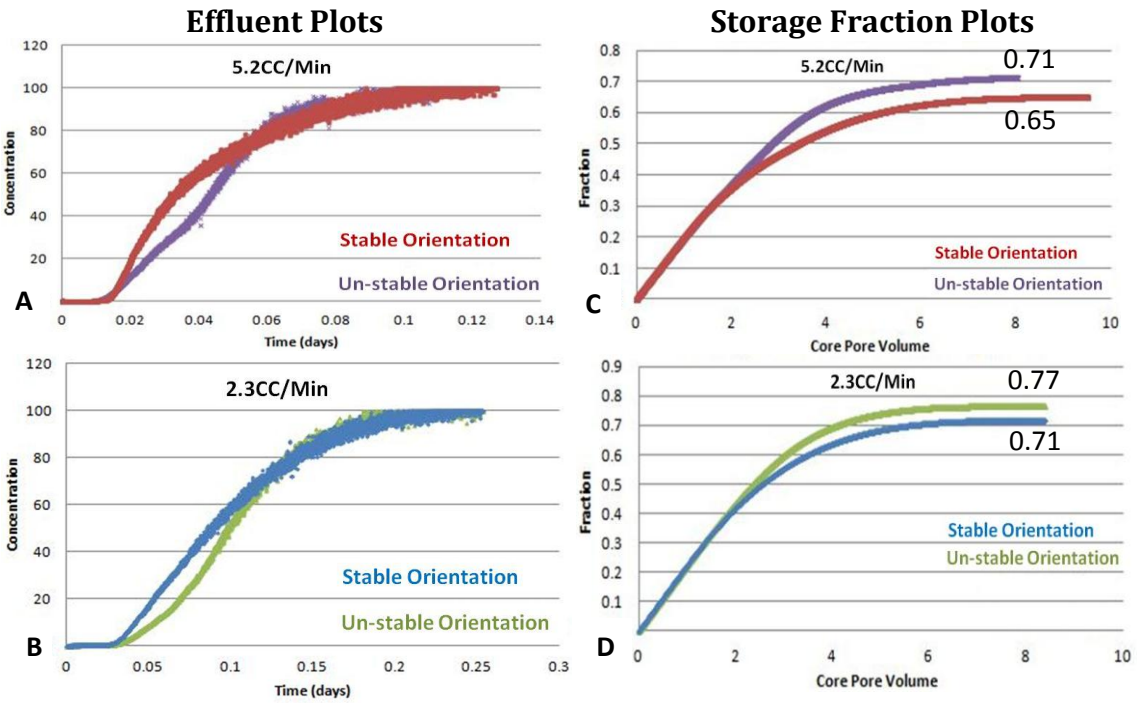

Figure 8. A and B are the arrival curves for CO_2 injected into air filled system in stable orientation and unstable orientation. In both cases curves for two flow rates, 5.2 cc/minute and 2.3 cc/minute are shown. The X axis is the duration of injection in days, and the Y axis is concentration of injected gas in the effluent. The arrival of the injected gas is delayed when it is injected in the unstable orientation. C and D are the storage fraction or sequestration plots for experiment A and B. The X axis is number of core pore volumes, and the Y axis is injected gas sequestered in the system expressed as a fraction of that which could be stored. The unstable orientation has the higher sequestration.

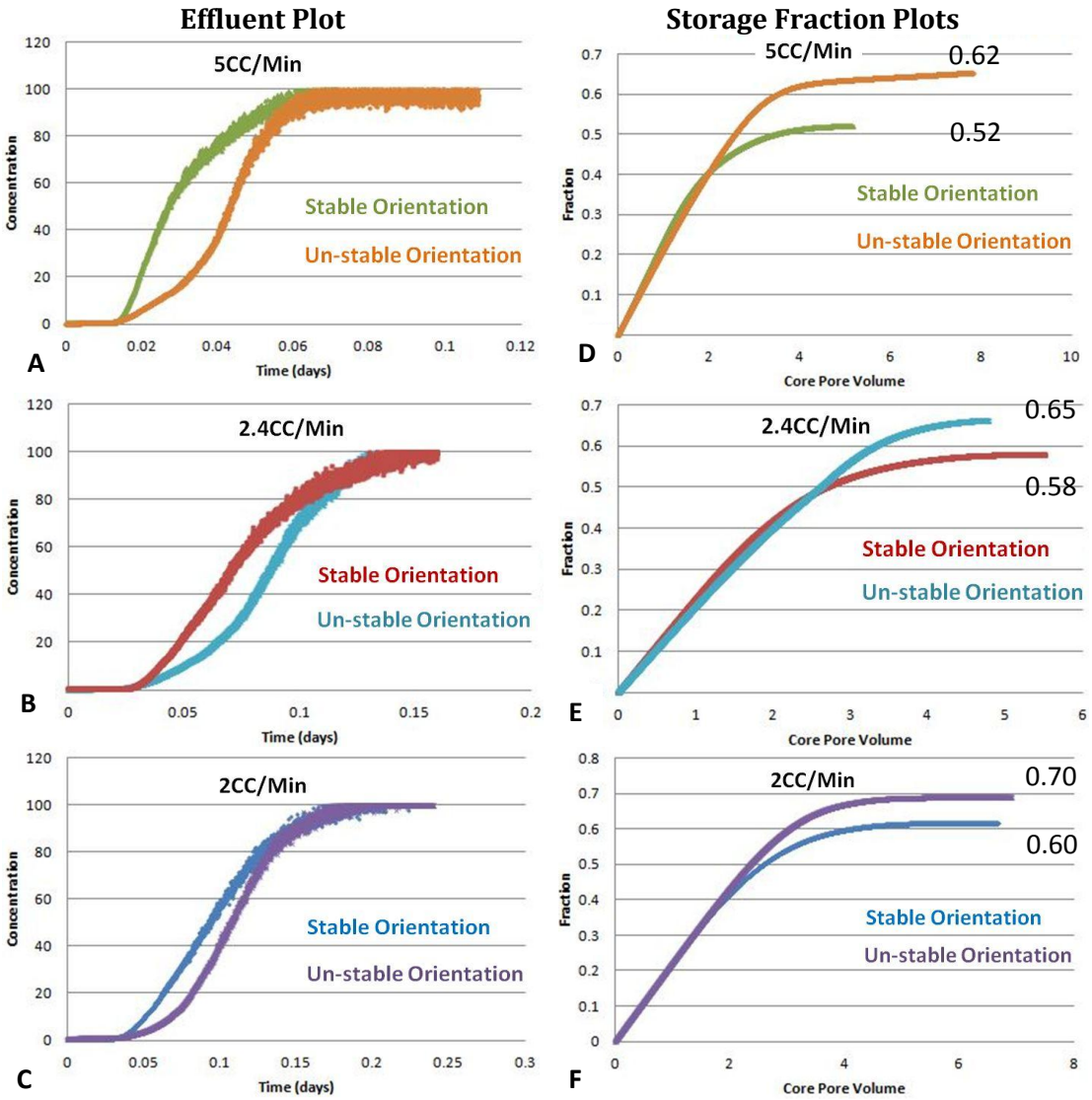

Figure 9. A, B and C are the arrival curves for CO_2 injected into a methane filled system in stable orientation and unstable orientation. The flow rate of A, B and C are 5, 2.4, and 2 cc/minute. Tin these plots the X axis is the duration of the injection in days, and the Y axis is the concentration of the injected gas in the effluent. The gas injected in the unstable orientation always experiences a greater delay in arrival. D, E and F are the storage fraction or sequestration plots for experiment A, B and C. The X axis is number of core pore volumes, and Y axis is the injected gas sequestered in the system expressed as a fraction of that which could be stored. The unstable orientation always corresponds to a higher sequestration.

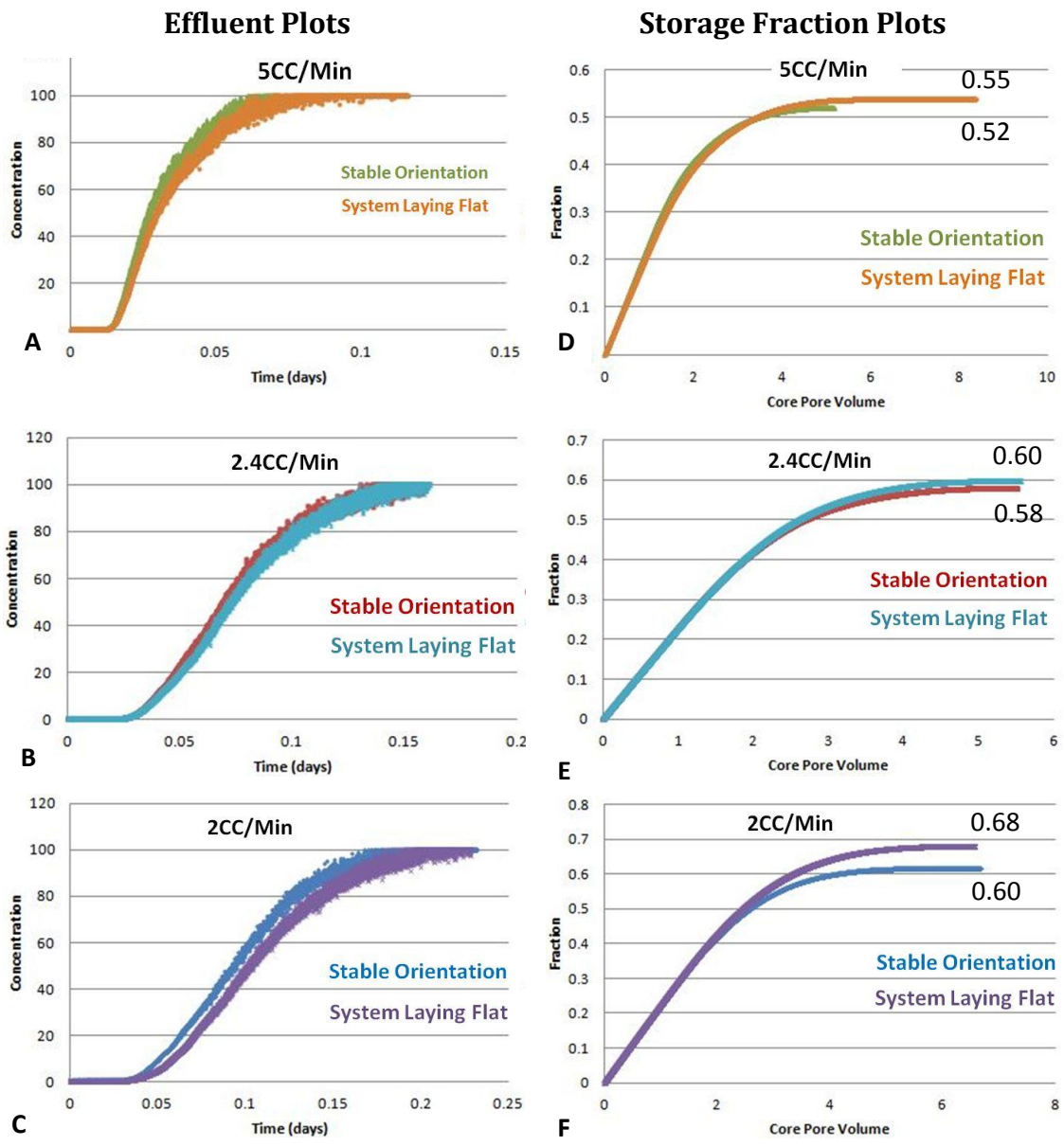

Figure 10. A, B and C are the arrival curves for CO_2 injected into a methane filled system in stable orientation and a horizontal orientation (the Hele-Shaw cell laying flat on the table). The flow rates in experiments A, B and C are 5, 2.4, and 2cc/minute respectively. The X axis is the injection duration in days, and the Y axis is the concentration of the injected gas in the effluent. The difference in effluent curves for these two orientations is very small, and the sequestration plots D, E and F show very similar CO_2 storage fraction.

Methane injected into a CO_2 filled vertical system

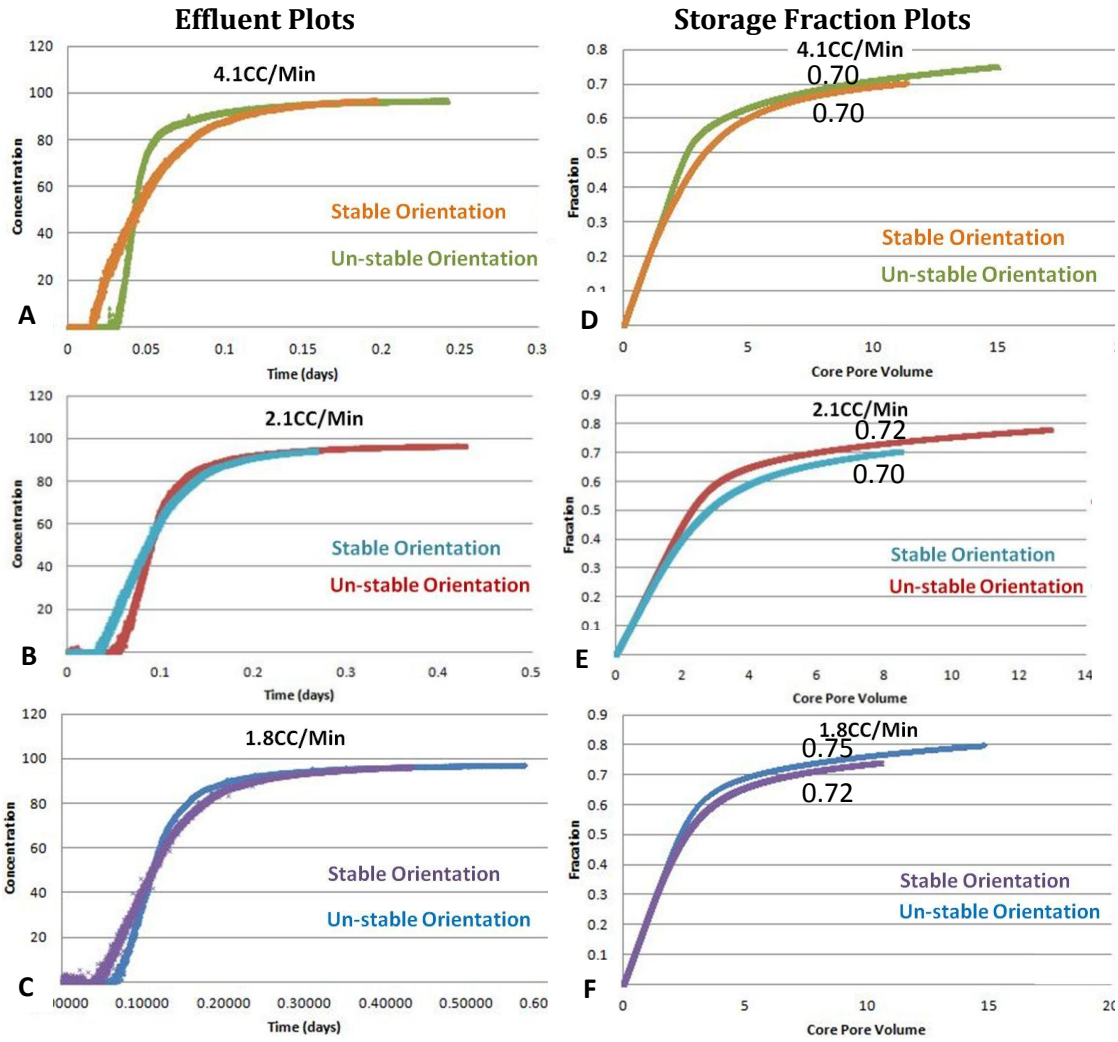

Figure 11. A, B and C are the arrival curves for methane injected into a CO_2 filled system in stable and unstable orientations. The flow rate of A, B and C are 4.1, 2.1, and 1.8 cc/minute respectively. The X axis is the duration in days, and the Y axis is the concentration detected for the injected gas in the effluent. A gas injected in the unstable orientation is again always delayed in its effluent arrival. D, E and F show that injection in the unstable orientation always sequesters more of the injected gas. The delay and increases in storage fraction or sequestration are, however, less than when CO_2 is injected into methane in an unstable orientation (Figure 9)

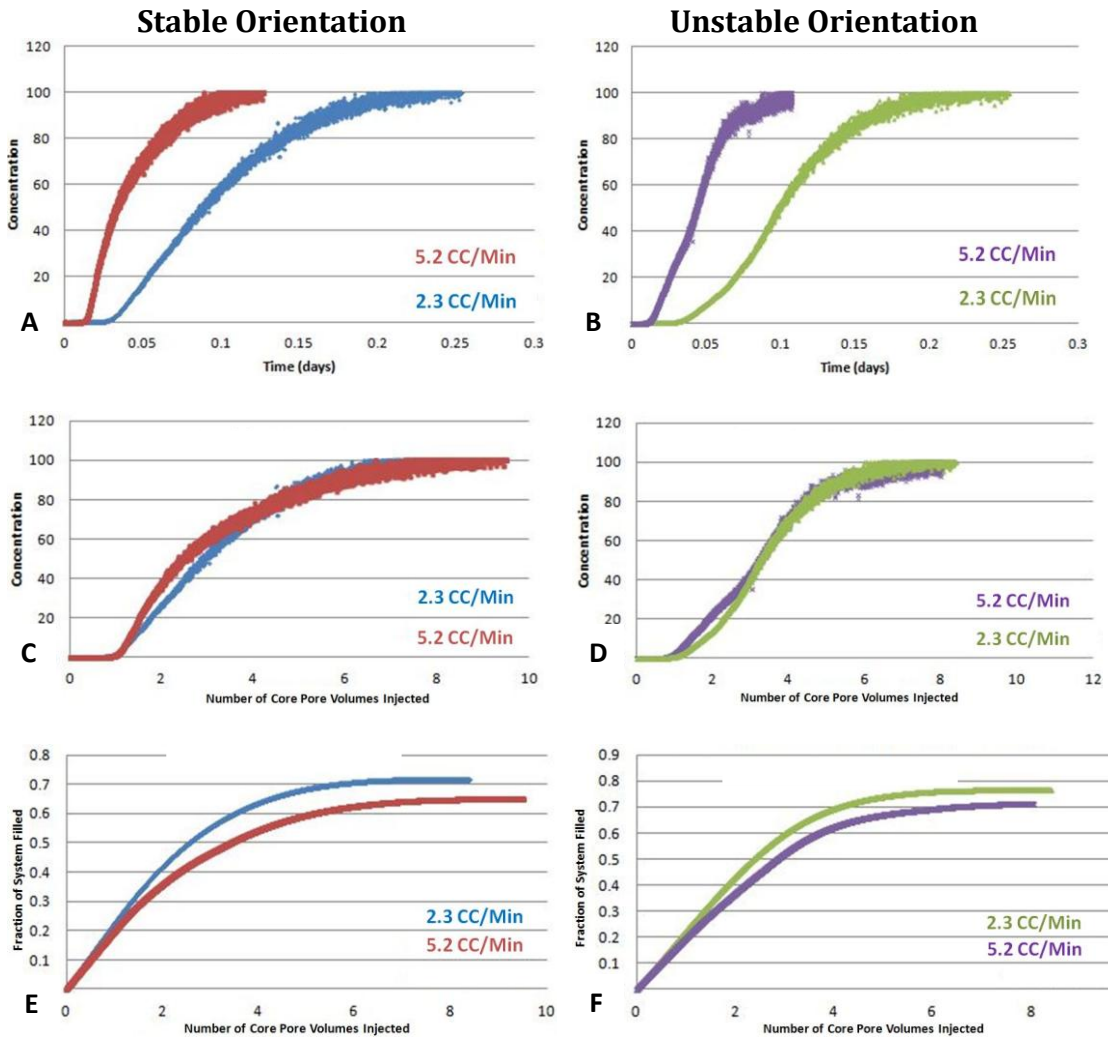

Figure 12. A and B are the arrival curves for CO_2 injected into an air filled system at flow rates of 5.2 and 2.3 cc/minute. The orientation of experiment figures in the left column are stable and figures in the right column are unstable. In figure A and B, the X axis is the duration in days, and the Y axis is the concentration detected for the injected gas in the effluent. Gas injected at higher flow rates arrives earlier in time, which is expected. C and D are the normalized arrival plots with injected volume. The X axis is number of core pore volumes, and the Y axis is still the concentration detected. We observe that slower flow rate experiments have a slight delay in arrival, which suggests that more injected gas has been stored in the system. E and F are the storage fraction for experiment A and B. The X axis remains the number of core pore volumes injected, and Y axis is the storage of the injected gas expressed as a fraction of that which could be stored. Slower flow rates have higher sequestration.

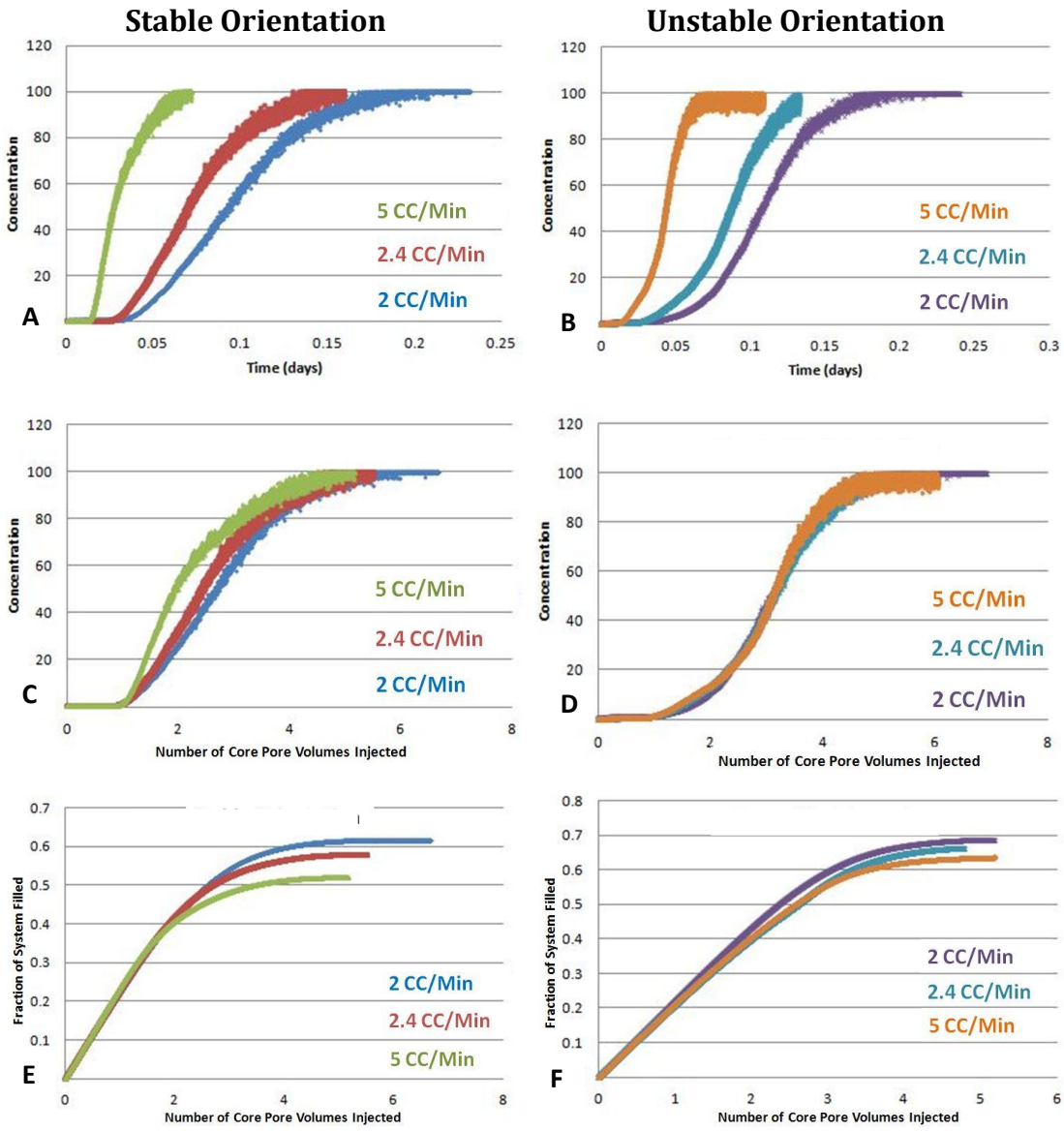

Figure 13. A and B plot effluent CO_2 as a function of time when CO_2 is injected into a methane filled system at 5 , 2.4, and 2cc/minute. The orientation of the experiment in the left column is stable and in the right column is unstable. In figure A and B, the X axis is the duration in days, and the Y axis is the concentration detected for the injected gas in the effluent. The gas injected at higher flow rate arrives faster, but C and D show that the arrival is similar when plotted as a function of the number of injected core pore volumes, especially for the unstable orientation (D). E and F show the storage fraction or sequestration is more for the slower flow rates in the stable configuration (E), but similar and fairly independent of flow rate for the unstable orientation (F).

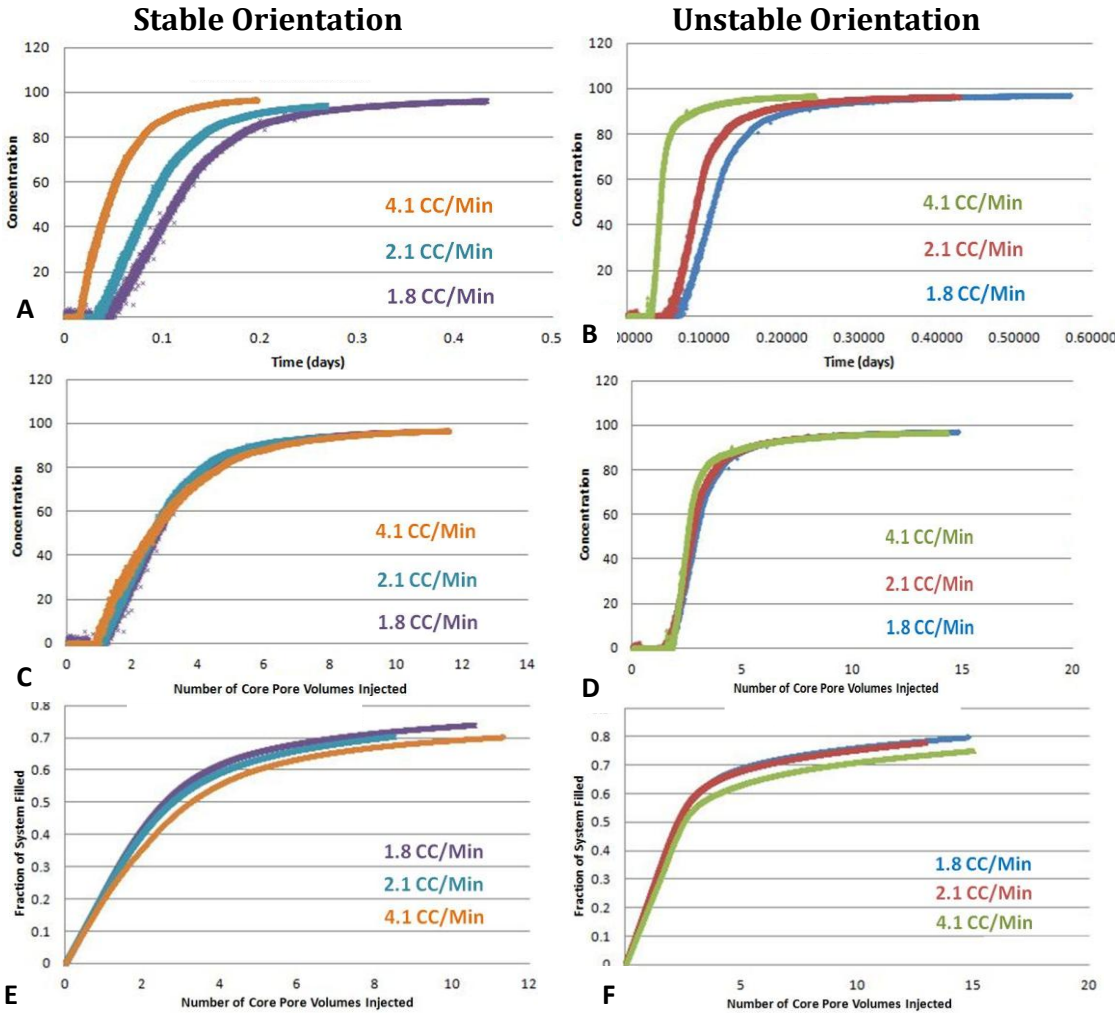

Figure 14. The experiments depicted in the left column are in stable orientation and those depicted in the right column are in unstable orientation. A and B plot effluent methane when methane is injected into a CO_2 filled system at rates of 4.1, 2.1, and 1.8 cc/minute, respectively. In figure A and B, the X axis is the duration in days, and the Y axis is the concentration detected for the injected gas. The gases injected at higher flow rates arrived sooner, but C and D shows they arrive at almost the same core pore volumes. The slower flow rate experiments have a slight delay in arrival, but the arrival curves have very similar form. The storage fraction plots show that the storage fraction is similar, with the slower flow rates showing only slightly greater sequestration.

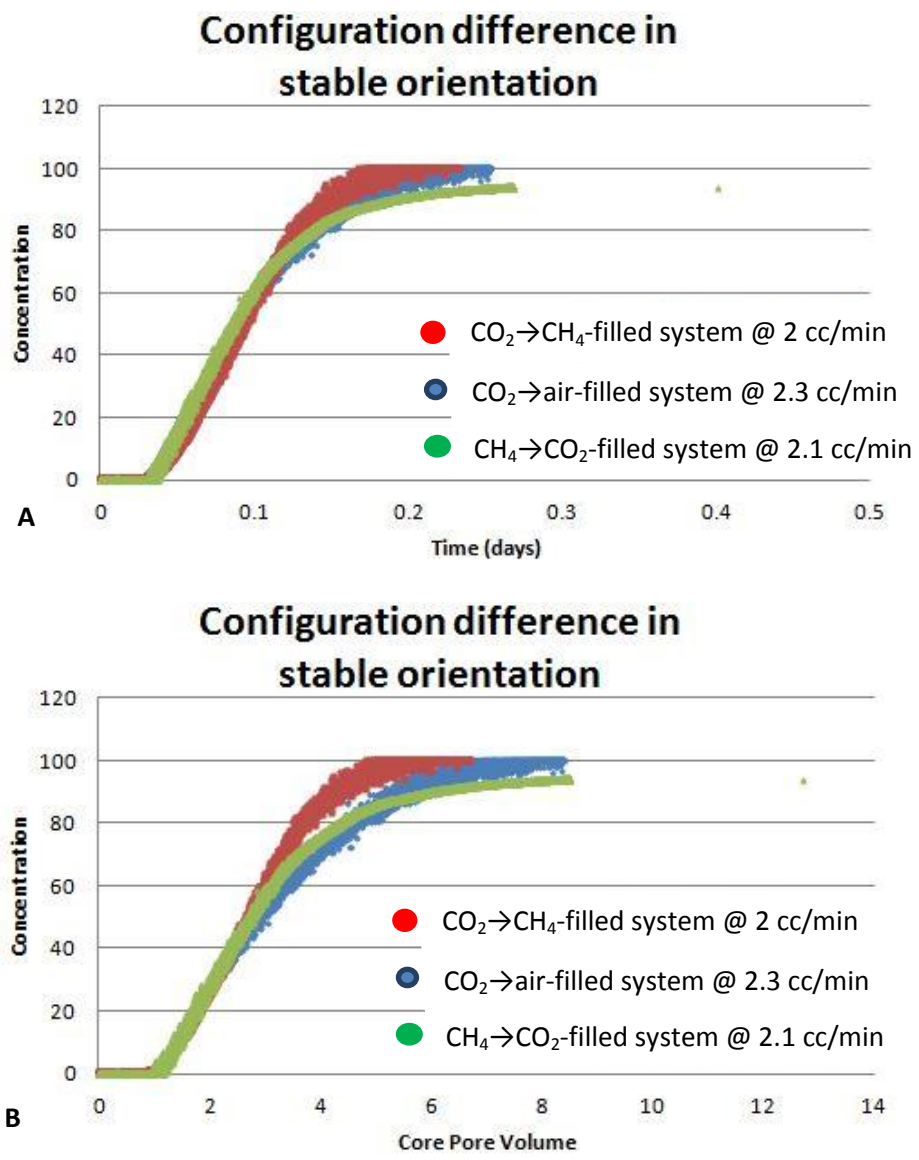

Figure 15: Effluent concentration plotted against (A) time and (B) core pore volumes for stable orientation. Three curves are shown in each figure: one for CO_2 injected into an CH_4-filled system, one for CO_2 injected into an air-filled system, and one for CH_4 injected into a CO_2 filled system. All injection rates of about 2 cc/minute. The effluent curves are quite similar, but there is some indication that the diffusion constant for CO_2 into a CH_4-filled system (red curve) may be less than for the other configurations.

CHAPTER 5

The Flow Model

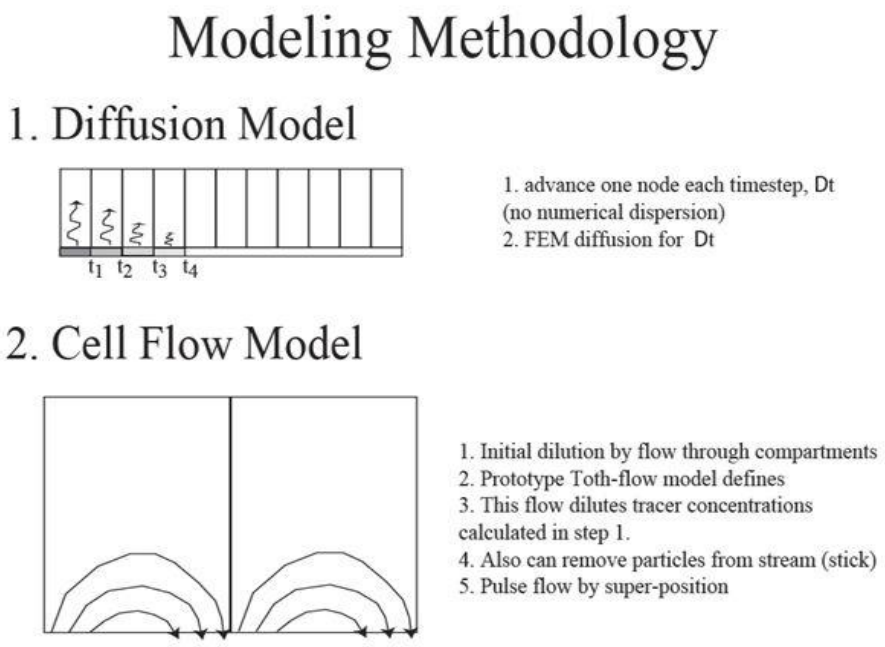

Figure 16: Diffusion model methodology.

The advection of tracer along the core channel and the diffusion of tracer into the slit are calculated separately with operator splitting methods. As Figure 16a shows, the core channel fluid is advanced in discrete time steps, after which the diffusion into the matrix is calculated using finite element methods. The longitudinal dispersion is calculated as the longitudinal coefficient a_L multiplied by the longitudinal velocity profile v_{co}. The transverse dispersion in the slit is calculated as $\left(\frac{a_T}{a_L}\right) a_L v_c$, where $\frac{a_T}{a_L}$ is the ratio of transverse to longitudinal

dispersion, usually around 0.1, and v_c is the horizontal velocity in the slit calculated as described below.

Toth's Flow Effect

Even if we subdivide our diffusion compartment into small segments, we still observe significant flow in each compartment. The flow expected in the slit compartments is shown in the Figure 16b above. There is a linear pressure drop across the core channel, and within each slit compartment this drives a circulation similar to that illustrated. We can calculate this flow using the methods of Toth (1959) and described in Subramanian et al. (2012). The gas flowing into the slit in each compartment will carry injected gas in, but the gas exiting the compartment will, for a while, contain none of the injected gas. Thus the circulation loops in each slit compartment dilute the gas moving through the core channel. We take this effect into account in our models. We calculated multiple streamlines in each compartment and track the flow along each one, diluting the channel until the flow along the streamline completes a loop from entry in to exit from the compartment. We found, however, that the model fit to the data in all the experiments was unchanged whether the flow in the compartment was considered of not.

Gaseous Diffusion Model Fits

The unstable orientation experiments are complicated by gravity induced circulation in the slit, and we therefore concentrate on modeling the experiments in the stable orientation.

CO_2 injected into an air filled system is modeled in Figure 17. The diffusion coefficient of CO_2 in air is between 0.14 and 0.177 cm^2/s (Pritchard 1982), and the best model fit of this set of experiments is with a diffusion coefficient equal to 0.18 cm^2/s. Longitudinal and latitudinal dispersion are minimal in Hele Shaw style flow. We used a very small value of a_L = 0.1mm and the ratio of transverse (latitudinal) to longitudinal dispersion of 0.1 in this and all subsequent cases. For these dispersion coefficients, dispersion does not affect the computed results.

Experiments where CO_2 is injected into a CH_4 filled system in stable orientations are modeled in Figure 18. The diffusion coefficient for CO_2 in CH_4 at 1 atm and 293K is 0.181 cm^2/s (Weissman and DuBro, 1971). Weissman and DuBro recommend using the laboratory measured values of the gas pair of interest if they are available because they are usually more accurate than values derived from empirical or semi-empirical equations. We adopted D_{12} with the value of 0.18 cm^2/s from Weissman and DuBro's work. , and correct this value with Chapman's empirical second-order approximation to take into account of differences in gaseous concentration. The second order diffusion correction for

these gases suggests D_{12}' should be increased by a factor of 1.045 which results in a diffusion constant of 0.19 cm^2/s. The best model fit is for a diffusion coefficient of 0.2 cm^2/s.

The model did not work well for CO_2 for this configuration and the model fits shown in Figure 18 were obtained by changing the width of the slit compartments in proportion to the flow rate through the core channel. The full constructed width of the slit is 28.5 cm. For a CO_2 injection rate of 2 cc/minute, the width was taken to be 22 cm, for 2.4 cc/minute, the width is 19 cm, and for 5 cc/minute, the width is 15 cm. As discussed below, we think that these changes are reasonable and reflect the stable layering of CO_2 in the slit. The changes in diffusion constant to achieve an equivalent fit would be unreasonably large. The best-fitting diffusion constant for this set of experiments with the modified slit widths is 0.18 cm^2/s.

The CH_4 injected into a CO_2 filled system in stable orientation is modeled in Figure 19. The best model fit is for a diffusion coefficient of 0.2 cm^2/s.

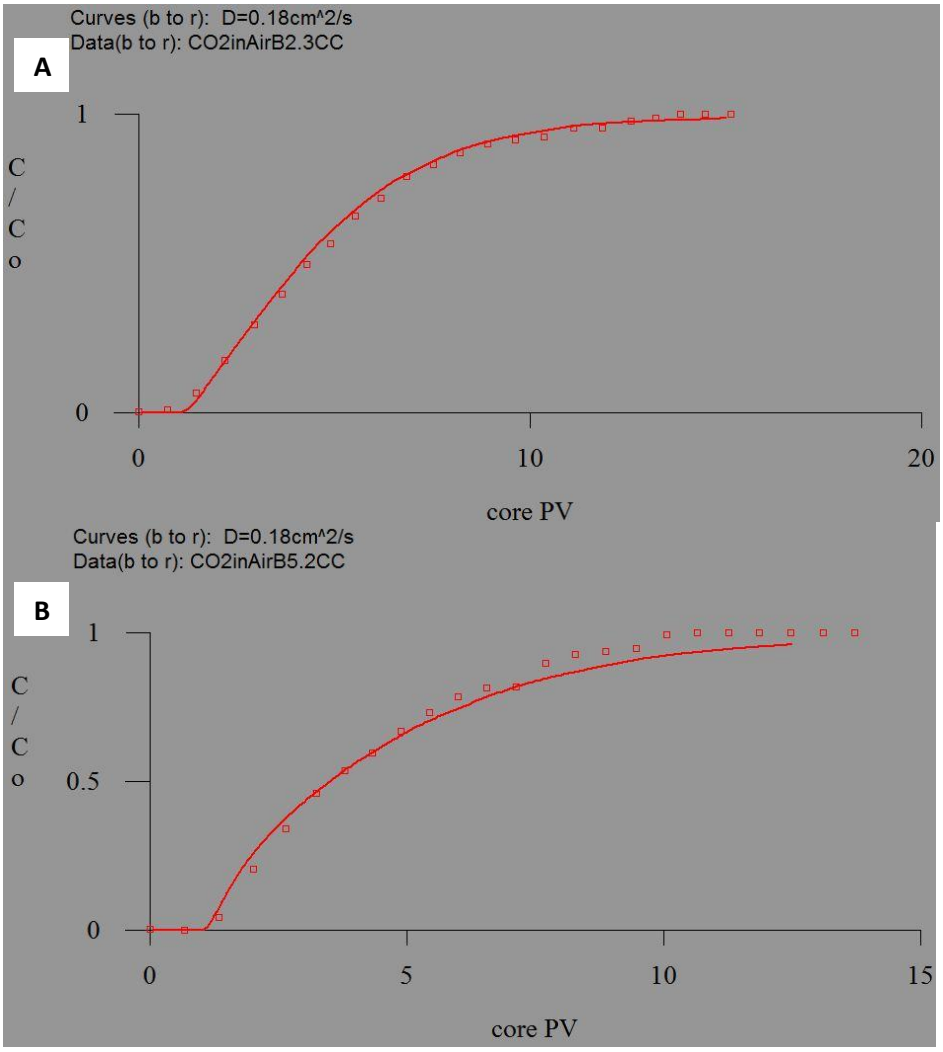

Figure 17. A) shows the model fit for CO_2 injected into an air filled system at 2.3 cc/minute with the cell in the stable orientation. The red solid line is the model's prediction, and the red squares are the experimental data points. The fit shown is for a diffusion constant of 0.18 $cm^2\ s^{-1}$. B) shows the model fit for CO_2 injected into an air filled system at 5.2 cc/minute. The solid curve is the effluent curve predicted for a diffusion constant of 0.18 $cm^2\ s^{-1}$.

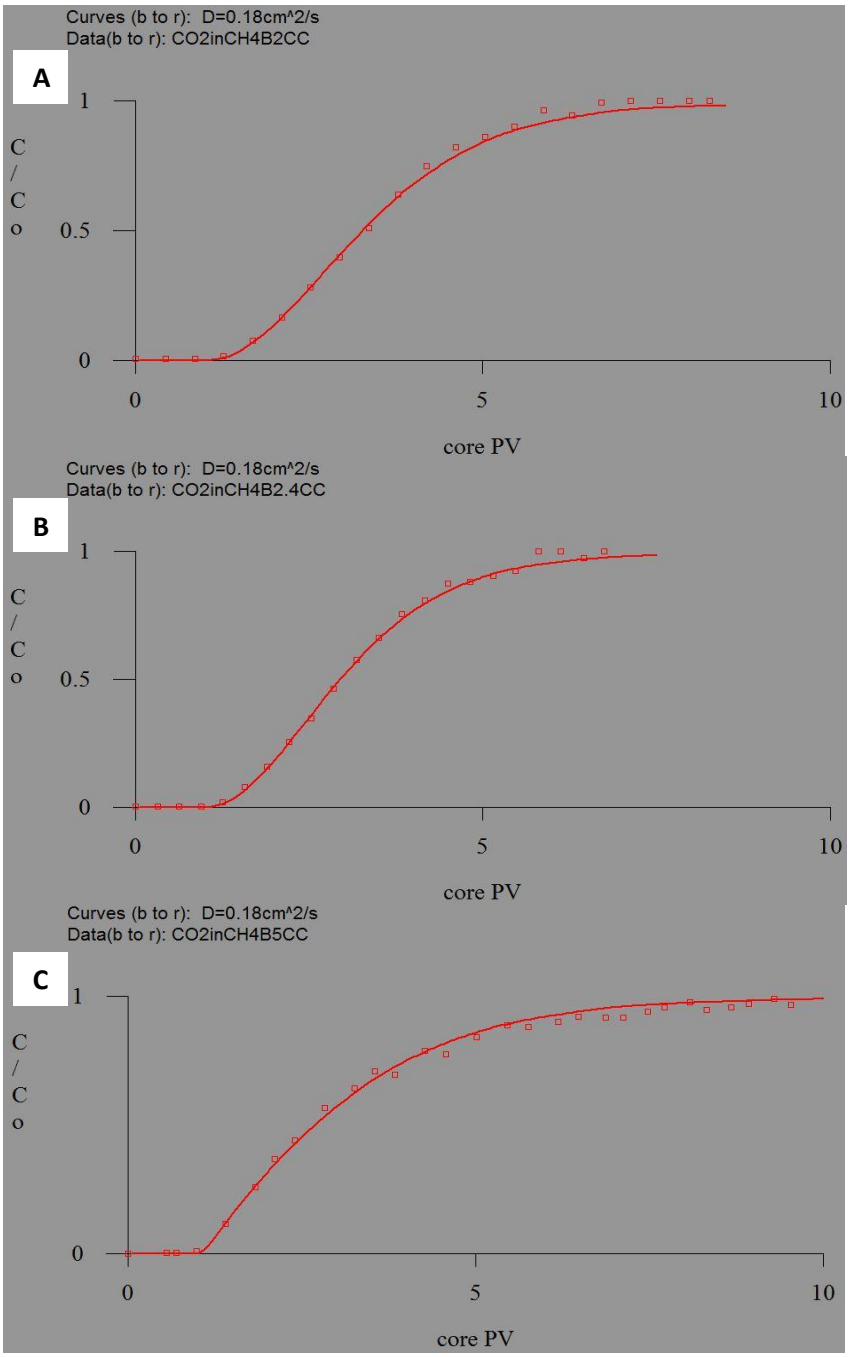

Figure 18. A) shows the model fit for CO_2 injected into a methane filled system at 2 cc/minute with the cell in the stable orientation. The red solid line is the model's prediction and the red squares are the experimental data points. The fit shown is for a diffusion constant of 0.18 cm^2 s^{-1} and a slit width of 22 cm. B) shows the model fit CO_2 injected into a methane filled system at 2.4 cc/minute. The solid curve is for a diffusion constant of 0.18 cm^2 s^{-1} and a slit width of 19 cm. C) shows the model fit for CO_2 injected into a methane filled system at 5 cc/minute. The solid curve is for a diffusion constant of 0.18 cm^2 s^{-1} and a slit width of 15 cm.

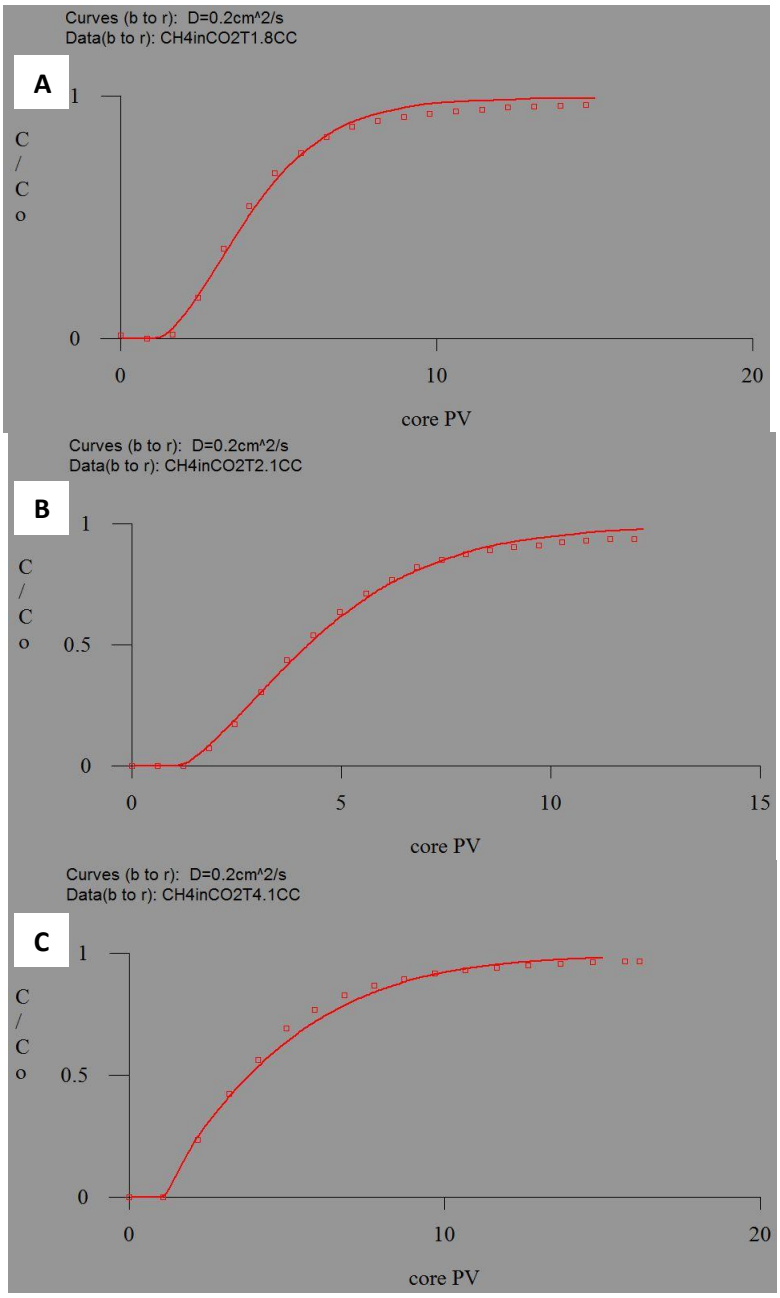

Figure 19. A) shows the model fit for methane injected into a CO_2 filled system at 1.8 cc/minute with the cell in the stable orientation. The red solid line is the model's prediction and the red squares are the experimental data points. The fit shown is for a diffusion constant of 0.2 $cm^2\ s^{-1}$. B) shows the model fit for methane injected into a CO_2 filled system at 2.1 cc/minute. The solid curve is the effluent curve predicted for a diffusion constant of 0.2 $cm^2\ s^{-1}$. C) shows the model fit for methane injected into a CO_2 filled system at 4.1 cc/minute. The solid curve is the effluent curve predicted for a diffusion constant of 0.2 $cm^2\ s^{-1}$.

CHAPTER 6

SUMMARY, DISCUSSION AND CONCLUSIONS

The experiments run show a good deal of internal consistency and indicate several clear and logical dependencies. As shown by Figures 8 to 11 and Table 2, sequestration is aided by gravity drainage in unstable orientations of the experimental apparatus. All unstable orientations have greater drainage. Diffusion enhances sequestration, and all experiments with slower injection rates show equal or greater storage of the injected gas. The greatest sequestration results when CH_4 is injected into a CO_2-filled system and the least sequestration results when CO_2 is injected into a CH_4-filled system. Gas diffusion makes less of a difference when CH_4 is injected into a CO_2-filled system in stable orientation (Figure 14), and diffusion seems to be slower for CO_2 injected into a CH_4-filled system.

The experiments can be modeled reasonably accurately using measured gas diffusion constants for the pairs of gases involved. Modeling CH_4 injection into CO_2 indicates a diffusion constant higher than the other cases (D=0.2 cm^2/s). Modeling CO_2 injected into an air-filled system indicates D=0.18 cm^2/s. Modeling CO_2 injected into a CH_4-filled system can be successfully accomplished with D=0.18 cm^2/s but requires adjustment of the width of the diffusion slit. The full constructed width of the slit is 28.5 cm. For a CO_2 injection rate of 2 cc/minute, the width was taken to be 22 cm, for 2.4 cc/minute, the width is 19 cm, and for 5 cc/minute, the width is 15 cm.

These observations and modeling results can potentially be explained by second-order diffusion effects and density stratification. If the injected gas is the high concentration gas, CH_4 injection into a CO_2-filled system should show the greatest diffusional sequestration (as observed) because, by Table 1, the non-linear diffusion enhancement is greatest in this case. Similarly, CO_2 injection into a CH_4-filled system should show the least diffusional sequestration (as observed) because, by Table 1, the non-linear diffusion enhancement is least in this case. The diffusional sequestration of CO_2 injected into an air –filled system should be almost as great as for CH_4 injected into CO_2 because the diffusional enhancement in this case is almost as great (Table 1). This is also observed (Table 2).

The low sequestration in the case of CO_2 injected into a CH_4-filled system may be also partly due to density stratification. Modeling of this case required adjustment of the width of the diffusion slit which could be a reflection of this stratification. Exactly how the stratification occurs and impacts the result is not clear. Under slower flow rates, diffusion has more opportunity to reduce the stratification and this may be why the greatest reduction in slit length was required for the faster flow rates. The correction is only needed for the densest and least dense combination, which also suggests gravity segregation as at least a partial explanation. Fitting the model to the data without adjustment of the slit width requires unreasonably large changes in the diffusion constant.

We always measure CO_2 concentration, and the error in measurement increases with the CO_2 concentration. This can be seen by the changes in the

width of the measurement band in the figures. For example, in the experiments where CO_2 is injected into air- or CH_4-filled system the data band increases as the effluent CO_2 concentration rises (e.g., Figure 8, 9). In the experiments where methane is injected into a CO_2-filled system, the effluent CO_2 concentration is initially 100% and declines with time and the data band is wide initially and then narrows (see Figures 11, 14, and 15). We average neighboring data points to determine the CO_2 concentration.

In some experiments the injected gas concentration plateaus at 97%-98% of the injected concentration, rather than 100%. This results in a false, nearly linear, rise in the storage fraction plots (see Figures 9a, 11 and 14). We selected the storage fractions summarized in Table 2 to avoid this effect as much as possible.

The diffusion constant used in our model for CH_4 injected into a methane-filled system was corrected by ~5% with Chapman's empirical second-order approximation, from 0.18 cm^2/s to 0.19 cm^2/s. The best model fit is for a diffusion coefficient of 0.2 cm^2/s. This correction assumes that the injected gas is the most abundant. At later times in an experiment this is expected multiple pore volumes of the injection gas flow through the core while the gas in the diffusion slit is progressively diluted. This is supported by the observation that our model fits the experimental data well at the beginning when the gases are in about equal concentrations without the second order diffusion coefficient correction, but the correction becomes progressively important with time as the slit gas is diluted

but the core gas is not. There is a clear suggestion that the second order diffusion constant corrections are important and gravity stratification may also be important in laboratory experiments. There is some suggestion that Chapman's corrections may be a bit too small, but given the uncertainties in the data and the complication of density stratification and compartment flow, of a more detailed interpretation than is given here is not warranted.

Gravity drainage into the diffusion slit (matrix) is important in the laboratory experiments, but is unlikely to be important in field applications. In the field only the inter-diffusion of gases will be important. Our experiments give some indication of why this will be the case. In the flat laying orientation when the core channel carries the heavier gas, that gas is ~8.7mm higher in elevation than the diffusion slit. When the apparatus is oriented at an un-stable orientation the column of heavier gas extends ~28.5 mm above the core channel. This change in orientation almost eliminates the gravity effects yet could be considered to be equivalent to a permeability reduction of ~3. At a few nanodarcies permeability the shale matrix will be at least 6 orders of magnitude less than the permeability of the fractures in the shale. Had the laboratory experiment had this large a permeability contrast between the slit and the channel, gravity flow into the slit and gravitational layering in the slit would have been completely unimportant. We are obliged to consider flow and gravity effects in the diffusion slit to interpret our laboratory experiments. They are of

no importance for the field applications of our results. In the field only gas inter-diffusion will be important.

Conclusions related to the laboratory experiments are: (1) A Hele Shaw-style apparatus can simulate the diffusional sequestration of CO2 that should occur as this gas is injected into a methane-filled shale. (2) Modeling of the Hele Shaw system experiments was successful using the gas inter-diffusion constant measured by others for the pairs of gases involved in our experiments of $\sim 0.18 cm^2/s$. (3) A second order correction of the diffusion constant was required for experiments involving the lightest and most dense gas pair (CH2 and CO2) when the lightest gas was the injected gas. The correction required was close to but a bit larger than that indicated by theory. (4) Gravity drainage and perhaps density stratification of the gases are important in the laboratory experiments. (4) But compartment flow is very small in our experiments and is not significant in their interpretation.

Inter-diffusion of gases is the key to CO_2 storage in shale. The implication of our experiments for sequestration of CO_2 in shale are: (1) The experiments run show, by analogy, how the inter-diffusion of injected CO_2 and ambient CH_4 in a gas shale can be modeled from the fracture spacing and porosity of the shale matrix. (2) The storage fraction plots shown to be so useful in interpreting the laboratory experiment should be an effective way to judge the viability of CO_2 storage from initial well tests. (3) The experiments suggest that storage of CO2 in gas shales could be feasible if the fracture spacing in the shale is small. For

more precise assessment, the methods developed in this thesis will need to be adapted to the field situation (fracture spacing, matrix porosity, diffusion constant of supercritical CO_2 with a density of ~600 kg/m^2 into methane with a density of ~200 kg/m^2, etc.).

APPENDIX A:

Flow Meter Operating Instructions:

1): Flow meter must always be oriented vertically to function correctly.

2): Close the valve by turning it clockwise - Do not over tighten

3): Pressurize the system (Do not exceed inlet pressure of 200psi. 15-20psi is adequate for this meter)

4): Open the valve until the float rises to the desired flow rate (note: flow meter may need to be adjusted periodically for the first 5-10 minutes until flow rate stabilizes.)

Fig. A1 – Correlated Flow Meter

Calibration Data – For STP: 1 atm @ 70°F

This information can be obtained by request through a Cole-Parmer representative.

Email requests can be sent to techinfo@coleparmer.com

Scale Reading	CO_2 Flow Rate (ml/min)	CH_4 Flow Rate (ml/min)
65	6.57	8.67
60	5.92	7.58
55	5.28	6.59
50	4.65	5.82
45	4.05	5.16
40	3.47	4.61
35	2.95	3.95
30	2.44	3.40
25	1.95	2.64
20	1.52	2.20
15	1.14	1.54
10	.840	1.10
5	.580	.439

Table A.1: Flow rate of injecting gas.

Fig. A2 – C20 CO_2 Sensor

The carbon dioxide sensor used for these experiments was obtained from CO2Meter.com. It is manufactured by Gas Sensing Solutions. The C20 is a real time sensor that can detect CO_2 concentrations from 0%-100%. It uses Aluminum Indium Antimonde NDIR (non dispersive infrared) LED technology. The sensor can be fitted with a tube cap that allows fluid to be injected across the sensor. The sensor is powered through a standard outlet and connects to a computer via USB. The software used to collect the data is called DAS100 and can be downloaded for free from the manufacturer's website.

A set of instructions along with a video for the DAS software can be found on the manufacturer's website.

REFERENCES

Busch, Andreas. Sascha Alles, Yves Gensterblum, Dirk Prinz, David N. Dewhurst, Mark D. Raven, Helge Stanjek, Bernhard M. Krooss. 2008. *Carbon dioxide storage potential of shales*. International Journal of Greenhouse Gas Control 2, 297-308

Carslaw, H. S., Jaeger, J. C., *Conduction of Heat in Solids*. Oxford at the Clarendon Press, Second Edition, 1959. ISBN 0198533683.

Cathles, L.M., R. Shannon. 2007. *How potassium silicate alteration suggests the formation of porphyry ore deposits begins with the nearly explosive but barren expulsion of large volumes of magmatic water.* Earth and Planetary Science Letters 262, 92-108

Cathles, L., H. Spedden, and E. Malouf, *A tracer technique to measure the diffusional accessibility of matrix block mineralization.* American Institute of Mining, 1974. 103rd Annual Meeting.

Chapman, S., and T. G. Cowling: "The Mathematical Theory of Non-Uniform Gases. An Account of the Kinetic Theory of Viscosity, Thermal Conduction and Diffusion in Gases", (3rd ed.), Cambridge University Press. 1970

Chen, N. H. and D. F. Othmer, *New Generalized Equation for Gas Diffusion Coefficient J. Chem. Eng. Data*, **1962**, *7* (1), pp 37–41. DOI: 10.1021/je60012a011

E. V. Evans and C. N. Kenney, *Gaseous Dispersion in Laminar Flow Through a Circular Tube Proc. R. Soc. Lond. A* 1965 **284**, 540-550. doi: 10.1098/rspa.1965.0079

Fong, H. H., Lee, J., Lim, Y., Zakhidov, A. A., Wong, W. H., Holmes, A. B., Ober, C. K., and Malliaras, G. G., *Orthogonal Processing and Patterning Enabled by Highly Fluorinated Light-Emitting Polymers*. Advanced Materials 2011, 23, p. 735-739. DOI: 10.1002/adma.201002986

Ghesmat, K., Hassanzadeh, H., Abedi, J., Chen, Z., *Influence of Nanoparticles on the Dynamics of Miscible Hele-Shaw Flows*. J. Appl. Phys. **109**, 104907 (2011); doi: 10.1063/1.3592228

Hirschfelder, J. O., C. F. Curtiss, and R. B. Bird: "Molecular Theory of Gases and Liquids," Wiley, New York, 1964.

Hudson, T. L., *PhD Thesis*, California Institute of Technology, 2008. Web only: http://resolver.caltech.edu/CaltechETD:etd-05022008-154254

Hwang, H. S., Lee, J., Zakhidov, A., DeFranco, J. A., Fong, H. H., Holmes, A. B., Malliaras, G. G., Ober, C. K., *Dry photolithographic patterning process for organic electronic devices using supercritical carbon dioxide as a solvent*. J. Mater. Chem., 2008, **18**, 3087-3090. DOI: 10.1039/b802713g

Krysmann, M. J., Kelarakis, A., Dallas, P., Giannelis, E. P., *Formation Mechanism of Carbogenic Nanoparticles with Dual Photoluminescence Emission.* J. Am. Chem.Soc. 2012, 134, 747-750

Marrero, T. R. and E. A. Mason, *Gaseous Diffusion Coefficient,* J. Phys. Ref. Data. Vol. 1, No. 1, 1972

McDowell-Boyer, L.M., J.R. Hunt, and N. Sitar, *Particle transport through porous media.* Water Resources Research, 1986. **22**(Copyright 1987, IEE): p. 1901-1921.

Nuttall, Brandon C. Cortland F. Eble, James A. Drahovzal. 2005. *Analysis of Devonian black shales in Kentucky for potential carbon dioxide sequestration and enhanced natural gas production.* Kentucky Geological Survey. Final Report DE-FC26-02NT41442

Paterson, Lincoln. 1981. *Radial fingering in a Hele Shaw cell.* Journal of Fluid Mechanics 113, 513-529

Pritchard, D.T., J.A. Currie. 1982. *Diffusion of coefficients of carbon dioxide, nitrous oxide, ethylene and ethane in air and their measurement*. Journal of Soil Science 33, 175-184

R. C. Reid and T. K. Sherwood. *The Properties of Gases and Liquids*, pages 2nd ed: 520–543, 632–633 4th ed: 577–597. McGraw-Hill Book Company, 1966, 1987.

Renner, T. A., *Measurement and Correlation of Diffusion Coefficients for CO_2 and Rich-Gas Applications.* SPE Reservoir Engineering. May 1988. p. 517-523

Saffman, P.G. and G. Taylor, *The Penetration of a fluid into a Porous Medium or Hele-Shaw Cell Containing a More Viscous Liquid.* Proceedings of the Royal Society A: Mathematical, Physical and Engineering Sciences, 1958. **245**(1242): p. 312-329.

Shapiro, A.M., *Effective matrix diffusion in kilometer-scale transport in fractured crystalline rock.* Water Resources Research, 2001. **37**(Compendex): p. 507-522.

Sherwood, T. K., Pigford, R. L., and C. R. Wilke: "Mass Transfer". McGraw-Hill Chemical Engineering Series. 1975, ISBN: 0070566925.

Silliman, S.E., *Particle transport through two-dimensional, saturated porous media: influence of physical structure of the medium.* Journal of Hydrology, 1995. **167**(1-4): p. 79-98.

Solomon, S., D. Qin, M. Manning, Z. Chen, M. Marquis, K.B. Averyt, M.Tignor and H.L. Miller. IPCC, 2007: *Climate Change 2007: The Physical Science Basis. Contribution of Working Group I to the Fourth Assessment Report of the Intergovernmental Panel on Climate Change.* Cambridge University Press, Cambridge, United Kingdom and New York, NY, USA.
S. K. R. Subramanian. *M.S. thesis*, Cornell University, 2011.

Subramanian, S. K., Li, Y., Cathles, L. M., *Assessing Preferential Flow by Simultaneously Injecting Nanoparticles and Chemical Tracers.* Water Resources Research, 2012, doi:10.1029/2012WR012148, in press.

Toth, J., *A Theory of Groundwater Motion in Small Drainage Basins in Central Alberta, Canada.* Journal of Geophusical Research, 1962. **67**(11).

Weissman, S., and G. A. DuBro, *Diffusion Coefficient for CO_2 -- CH_4.* J. Chem. Phys. **54**, 1881(1971); doi: 10.1063/1.1675111.